Battery Operated Soft Switching Resonant Buck–Boost LED Driver With Single Magnetic Element

Farhad Pouladi, Hosein Farzanehfard, and Ehsan Adib

***Abstract*—A simple buck–boost LED driver suitable for battery operated applications with limited input voltage level is presented in this paper. Soft switching performance is provided for the main switch via a resonant circuit to improve the converter efficiency. The incorporated auxiliary switch also performs under zero voltage switching condition. Both power switches can be driven with a simple gate drive circuit, so, the additional switch does not add any driving complexity. In addition, only one magnetic element is utilized in the proposed LED driver which contributes to circuit simplicity and lower weight and size. Also, all diodes turn OFF at zero current switching which eliminates the reverse recovery losses and improves efficiency. A laboratory prototype converting 12 V input voltage to 32 V output operating at 26 W output power is implemented and tested to verify the effectiveness of the proposed LED driver.**

***Index Terms*—Buck–boost, coupled inductors, LED driver, resonant circuit, soft switching.**

I. Introduction

ILLUMINATING sector forms a considerable share of energy consumption, so, emerging new energy efficient illuminating technologies is much appreciated. LEDs seem to be proficient solution in diverse illuminating applications due to their compact size, higher efficiency, environment friendliness, and higher lighting efficiency. As a result, LEDs are pervasively being employed in different lighting systems from traffic lights, automobile, and home lighting to displays of portable electronic devices and TV screens [1].

LEDs need to be fed by a constant current and their brightness can be controlled by their average forward current [2]. Thus, a dc–dc switching power converter is necessary to provide the required regulated current for LEDs. Tailored to the application, LEDs are usually connected in series and parallel configurations to satisfy the lighting requirements [3]. Due to the vast emerging portable electronic devices and applications, a wide area of novel LED applications including battery-driven or

Manuscript received January 31, 2018; revised April 29, 2018; accepted May 29, 2018. Date of publication June 13, 2018; date of current version February 5, 2019. This work was supported by SPAA05.com Company from the Netherlands. Recommended for publication by Associate Editor M. Ponce-Silva. *(Corresponding author: Hosein Farzanehfard.)*

The authors are with the Department of Electrical and Computer Engineering, Isfahan University of Technology, Isfahan 84156-83111, Iran (e-mail:

battery voltage is low. However, two magnetic cores are utilized which increase circuit volume. A two channel LED driver is proposed in [18] with integrated half bridge-boost structure and coupled inductors. Current uniformity is automatically obtained by a simple dc-blocking capacitor, and zero voltage switching (ZVS) operation is achieved for both switches. In addition, the drive structure is extendable and multiple LED channels can be driven. However, the applied series dc blocking capacitor reduces the converter gain and therefore to achieve the required voltage gain, high turn ratio of coupled inductors is necessary. Also, the power is processed twice since boost and half bridge converters are in series. A two phase interleaved LED driver is presented in [19] with reduced input current ripple which is desirable for the input battery lifetime. But the large series electrolyte capacitor employed in the power path can reduce the converter lifetime and efficiency. Also, switches perform under hard switching condition, and two separate magnetic cores are employed that increase circuit weight and volume. A buck–boost dc–dc converter topology is introduced in [20] in which soft switching performance is provided for all active elements, however, three switches are employed and resonant capacitor voltage stress is relatively high.

In this paper, a buck–boost soft switching LED driver suitable for battery operated purposes is proposed. One magnetic element is adopted which decreases the circuit volume. The proposed converter can perform both in boost and buck modes, so it has the flexibility to drive LEDs with different colors. Also, when LEDs are cold, the total required forward voltage may exceed the battery voltage level, and when they are warm, the forward voltage can be decreased to below battery voltage level. In such cases, having simultaneous buck and boost capabilities is highly valuable. In addition, the circuit structure is such that both switches can easily be driven with a simple gate-driver by adopting a P-MOS as the auxiliary switch, so, the additional power switch does not add any driving circuit complexity. Moreover, additional LED string can be driven by adding a third winding to the coupled inductors core.

The rest of this paper is organized as follows. In Section II, the proposed circuit is introduced and its structure and operating principles are explained. The steady state analysis and design guideline are covered in Section III. In Section IV, the control method is discussed and a thorough performance comparison between the proposed converter and other counterparts is provided in Section V. Section VI deals with the experimental results and finally, conclusions are discussed in Section VII.

II. Proposed Buck–Boost LED Driver

The proposed LED drive converter is shown in Fig. 1. This converter is derived by applying some modifications on the basic buck converter. The buck converter inductor is replaced with coupled inductors. The secondary winding of the coupled inductors is placed in series with the output diode. A resonant circuit is added in series with the primary winding containing a resonant capacitor C_r and a power switch in parallel with the capacitor. As a result, soft switching condition is provided and the converter can perform both in buck and boost modes. If the auxiliary switch remains OFF at all times, the converter operates in the buck mode, and if it performs alongside the main switch, the converter operates in the boost mode. Thus, the proposed converter can be employed in battery operated LED applications where the total forward voltage tolerance of LED strings may fluctuate due to temperature changes of LEDs.

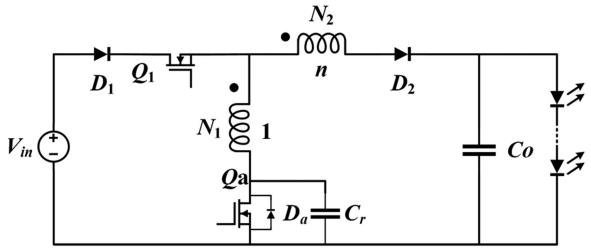

Fig. 1. Proposed boost type LED driver.

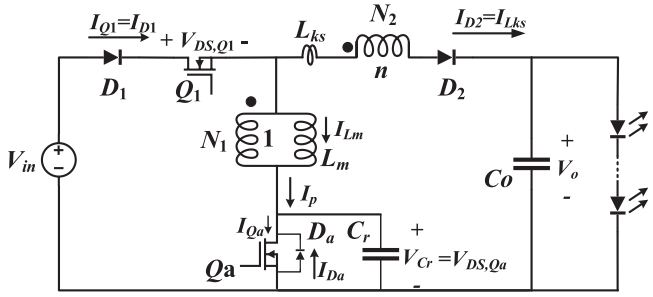

Fig. 2. Equivalent circuit of the proposed LED driver.

The equivalent circuit of the proposed LED driver is illustrated in Fig. 2, in which, the coupled inductors are modeled by an ideal transformer with primary and secondary windings N_1 and N_2, a magnetizing inductance L_m, and equivalent secondary leakage inductance L_{ks}. The main switch is Q_1, which is unidirectional in current through the input diode D_1, C_r is the resonant capacitor, Q_a is the auxiliary switch, D_a is the auxiliary switch anti-parallel diode, D_2 denotes the output diode, and C_o is the output capacitor. At steady state, the proposed converter has six different operating modes which are explained as follows. The main waveforms of the proposed LED driver are shown in Fig. 3, and the current path of the converter in each operating mode is depicted in Fig. 4. To simplify the converter analysis, all semiconducting elements are considered ideal and the output capacitor is large enough so that its voltage can be assumed constant in a switching cycle. Prior to the first operating mode, all semiconducting elements are in OFF state and the output load is being fed by the output capacitor.

Mode 1 (t_0, t_1): This mode begins by turning Q_1 and Q_a ON at ZCS due to the leakage inductance. D_1 is conducting while D_2 is reverse biased. The magnetizing inductance current I_{Lm} increases linearly as described by (1). This mode ends when Q_a is turned OFF

$$I_{Lm}(t) = \frac{V_{\text{in}}}{L_m} t. \tag{1}$$

The initial condition of the magnetizing inductance current needed for the next mode can be calculated as below

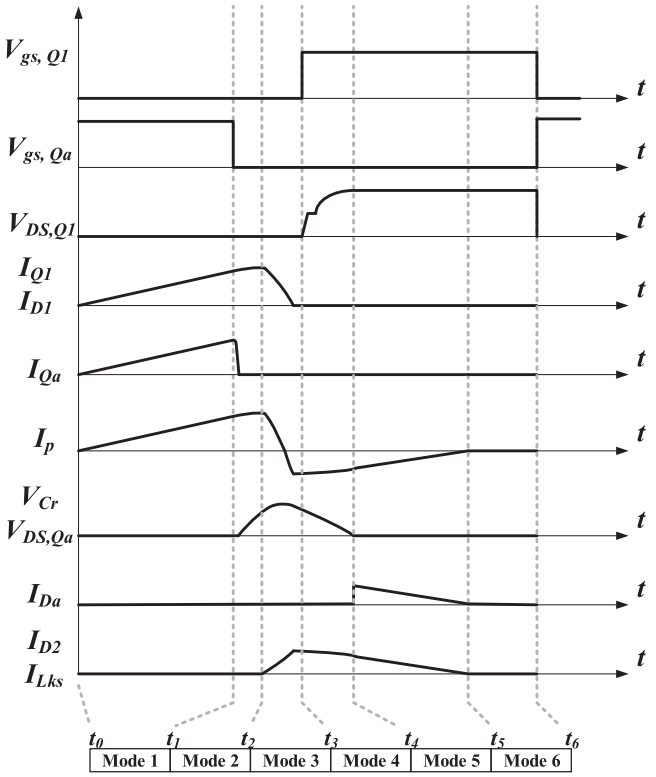

Fig. 3. Main waveforms of the proposed LED driver.

$$I_{Lm}(t_1) = \frac{V_i}{L_m} t_1 = I_1. \tag{2}$$

Mode 2 (t_1, t_2): At t_1, Q_a turns OFF under ZVS due to C_r. A resonance starts between L_m and C_r, which increases the C_r voltage (V_{Cr}) and this mode ends when D_2 starts to conduct. The following equations are obtained for this mode:

$$I_{Lm}(t) = C_r \omega_1 V_{\text{in}} \sin[\omega_1 (t - t_1)] + I_1 \cos[\omega_1 (t - t_1)] \tag{3}$$

$$V_{Cr}(t) = V_{\text{in}} \left[1 + \omega_1 t_1 \sin[\omega_1 (t - t_1)] - \cos[\omega_1 (t - t_1)]\right] \tag{4}$$

$$\omega_1 = \frac{1}{\sqrt{C_r L_m}}. \tag{5}$$

Mode 3 (t_2, t_3): At t_2, the C_r voltage increases to a point that forward biases D_2. The current increment in D_2 is gradual because of L_{ks} and the C_r voltage is still increasing. The current through Q_1 is declining while the coupled inductor secondary side current is rising. Then the primary side current changes its direction and increases until it reaches L_{ks} current while C_r voltage is declining. At the end of this mode, Q_1 current descends to zero and this mode ends. The main equations of this mode are as below, considering $n^2 L_m >> L_{ks}$

$$V_{Cr}(t) = \frac{L_{ks} \omega_2 I_1}{n^2} \sin[\omega_2 (t - t_2)] + \frac{V_o + (n-1) V_{in}}{n} \tag{6}$$

$$I_{Lm}(t) = I_2 - \frac{L_{ks} I_2}{n^2 L_m} \left[1 - \cos[\omega_2 (t - t_2)]\right] - \frac{V_o - V_{in}}{n L_m} (t - t_2) \tag{7}$$

$$\omega_2 = \frac{n}{\sqrt{C_r L_{Ks}}} \tag{8}$$

where I_2 is the initial condition for L_m in this mode, and is approximately equal to I_1 due to large value of L_m and short duration of the second mode.

Mode 4 (t_3, t_4): At t_3, D_1 current reaches to zero and D_1 turns OFF at ZCS and the associated reverse recovery problem is removed. Also, Q_1 is turned OFF under ZCS condition and switching losses are decreased. The resonance between C_r, L_m, and L_{ks} continues until C_r voltage reaches zero at the end of this mode. The change in current direction of primary side and ZCS turn OFF of the switch occur almost at the same moment because secondary leakage current is relatively large and its current is almost zero at the end of this mode. The following equations are established through this mode:

$$\omega_3 = \frac{1}{(n-1)\sqrt{L_m C_r}} = \frac{\omega_1}{(n-1)} \tag{9}$$

$$I_{Lm}(t) = I_3 \cos[\omega_3 (t - t_3)] + \sqrt{\frac{C_r}{L_m}} (V_3 - V_o) \sin[\omega_3 (t - t_3)] \tag{10}$$

$$V_{Cr}(t) = (V_3 - V_o) \cos[\omega_3 (t - t_3)] - \sqrt{\frac{L_m}{C_r}} I_3 \sin[\omega_3 (t - t_3)] + V_o. \tag{11}$$

In which I_3 and V_3 are the initial conditions of L_m and C_r at t_3 which are calculated by considering $t = t_3$ in equations (7) and (6), respectively

$$I_3 = I_{Lm}(t_3) = \frac{n-1}{n} I_1 \tag{12}$$

$$V_3 = V_{Cr}(t_3). \tag{13}$$

Mode 5 (t_4, t_5): At t_4, the voltage across C_r reaches zero and Q_a antiparallel diode D_a starts to conduct. The output voltage is applied across L_m and L_{ks} and their current decreases linearly to zero by the end of this mode. Following equations can be obtained for this mode:

$$V_{Cr}(t) = 0 \tag{14}$$

$$I_{Lm}(t) = I_4 - \frac{V_o}{(n-1) L_m} (t - t_4). \tag{15}$$

In which I_4 is the initial condition of L_m at the beginning of this mode which is obtained from (10) in the fourth mode at $t = t_4$

$$I_4 = I_{Lm}(t_4). \tag{16}$$

Mode 6 (t_5, t_6): At t_5, L_m current becomes zero and D_a along with D_2 turn OFF under ZCS condition, so their reverse recovery problem is alleviated. All semiconductor devices are in OFF state, and the LED load is supplied by the output capacitor.

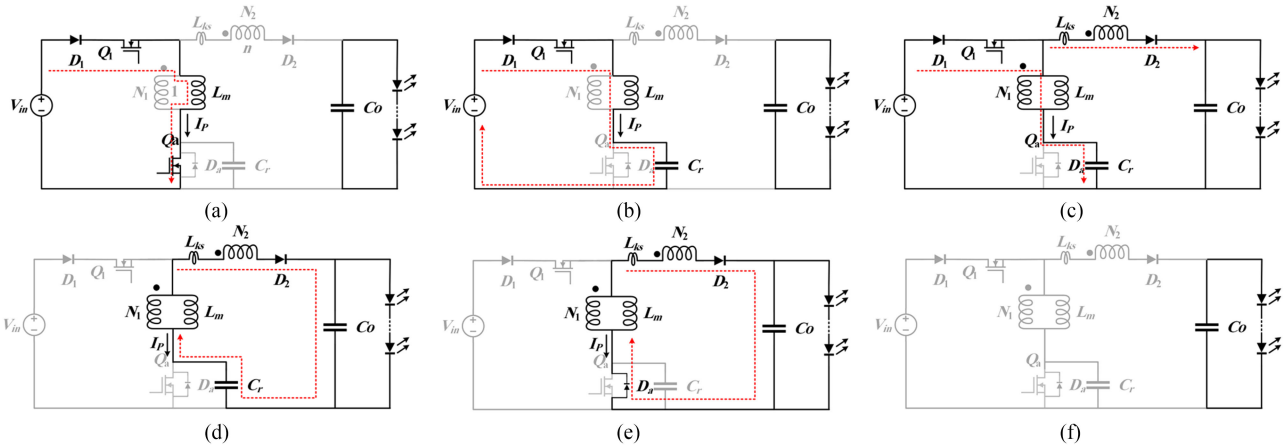

Fig. 4. Operating modes of the proposed converter. (a) Mode 1. (b) Mode 2. (c) Mode 3. (d) Mode 4. (e) Mode 5. (f) Mode 6.

L_m current and C_r voltage are zero throughout this mode. Next switching cycle begins when Q_1 and Q_a are turned ON.

III. Steady State Analysis

In this section, the design procedure of the proposed converter is presented.

A. Designing the Magnetizing Inductance

When both switches are conducting, V_{in} is applied across L_m and the energy stored in L_m can be obtained as below

$$E_{Lm} = \frac{1}{2} L_m I_{Lm}^2 \tag{17}$$

$$E_{Lm} = \frac{1}{2} L_m \left(\frac{V_{\text{in}}}{L_m} D_{Qa} T \right)^2 \tag{18}$$

where D_{Qa} is the duty cycle of the auxiliary switch. When Q_a is turned OFF, a resonance occurs between L_m and C_r which transfers L_m energy into C_r. Also, additional energy is absorbed during this resonance which can be neglected since resonance duration is very small in comparison to $D_{Qa}T$. This energy then is transferred to the output by C_r. So, the stored energy in L_m multiplied by the switching frequency is almost equal to the power delivered to the output

$$\frac{1}{2} L_m \left(\frac{V_{\text{in}}}{L_m} D_{Qa} T \right)^2 f = P_{\text{out}} = \frac{V_o^2}{R_o} \tag{19}$$

$$L_m = \frac{V_{\text{in}}^2 D_{Qa}^2 R_o}{2 f V_o^2}. \tag{20}$$

B. Selecting Coupled Inductors Turns Ratio

The maximum voltage of C_r can be extracted from mode 3 as below

$$V_{Cr-\max} = \frac{I_1}{C_r \omega_2} + \frac{V_o + (n-1)V_{\text{in}}}{n} \tag{21}$$

where I_1 can be calculated from (2). At the end of third mode, t_3, the primary side current, which is the same as C_r current but in reverse direction, equals to the secondary side current, so the following equations can be obtained:

$$I_{Lks}(t_3) = -I_{Cr}(t_3) \tag{22}$$

$$I_{Lks}(t) = \frac{I_1}{n}(1 - \cos[\omega_2 (t - t_2)]) \tag{23}$$

$$I_{Cr}(t) = I_1 \cos[\omega_2 (t - t_2)]. \tag{24}$$

By substituting (23) and (24) into (22), following equation is extracted:

$$\cos(\omega_2 t_3) = \frac{1}{1-n}. \tag{25}$$

From (25) it can be derived that *n* should be selected greater than 2.

L_m is discharged during the fifth mode in a linear manner. From (15), in order for L_m to be fully discharged, following condition should be satisfied:

$$\frac{V_o}{(n-1)L_m} t \geq I_4. \tag{26}$$

Duration of the fifth mode should be designed in a way that L_m has enough time to be discharged. Hence, duration of the fifth mode is designed to be almost equal to a quarter of switching period. Further reduction in the duration of this mode results in high current peak of the output diode. Also, I_4 is almost equal to I_3 which is calculated from (12). So, (26) can be rewritten as

$$\frac{V_o}{(n-1)L_m} \times \frac{T}{4} \geq \frac{n-1}{n} I_1. \tag{27}$$

By doing some simplifications, the upper limit for *n* can be obtained as (28). Regarding the fact that this upper limit is calculated for the designed values of I_1 and fifth mode duration and should be recalculated for other desired design scenarios

$$n \leq \frac{2 + A + \sqrt{A^2 + 4A}}{2} \tag{28}$$

$$A = \frac{V_o T}{4 I_1 L_m}. \tag{29}$$

Also, looking at (11), since the amplitude of the first term is much smaller than the amplitude of the second one, the

following equation should be satisfied for complete discharge of C_r:

$$\sqrt{\frac{L_m}{C_r}} I_3 \sin[\omega_3 (t - t_3)] > V_o. \tag{30}$$

Substituting I_3 from (12) in (30), and also using (5), (30) can be rewritten as below, and another limit for *n* is achieved

$$L_m \omega_1 \frac{n-1}{n} I_1 > V_o \tag{31}$$

$$n > \frac{L_m \omega_1 I_1}{L_m \omega_1 I_1 - V_o}. \tag{32}$$

C. Designing Resonant Capacitor

A switching period consist of six different time intervals from t_0 to t_6 as below

$$T = t_{01} + t_{12} + t_{23} + t_{34} + t_{45} + t_{56} \tag{33}$$

in which t_{mn} is $t_n - t_m$. t_{01} is the time through which L_m is charged and is decided based on the output power and is the same as $D_{Qa}T$, and is considered about 40% of the switching period, T_{sw}. Resonance takes place during intervals t_{12}, t_{23}, and t_{34} by which ZCS condition is provided for the main switch. This resonance should happen very fast, hence, the frequency of these three resonances should be designed to be about ten times of the switching frequency. Thus, the total duration of resonances can be designed to be about 10% of T_{sw}. C_r is charged during t_{12} and t_{23}, then is discharged during t_{34} from its peak value to zero. t_{45} is the interval in which L_m is discharged linearly and is designed about a quarter of the switching period. Finally a guard time, t_{56} is considered to ensure the mentioned processes are completed, and can be designed between 15% and 30% of T_{sw}.

C_r should be discharged to zero from approximately its peak to zero value during the fourth mode. So, equalizing (11) with zero and doing some simplifications would result in

$$\sin(\omega_3 t_4) = \frac{n V_o}{I_1 (n-1)} \sqrt{\frac{C_r}{L_m}}. \tag{34}$$

From (9) ω_3 is calculated, and with the assumption that C_r is discharged from its peak value to zero during t_{34}, as well as considering total duration of resonances to be about $0.1T_{\text{sw}}$, t_{34} is approximately $0.05T_{\text{sw}}$. Hence, C_r can be calculated from (35) where I_1 is obtained from (2)

$$C_r = \frac{\left[(n-1)\sin(\omega_3 t_4) I_1\right]^2 L_m}{(n V_o)^2}. \tag{35}$$

D. Voltage Gain

The proposed converter operates in DCM mode, and its voltage conversion ratio can be calculated by equalizing the output power with the power stored and transferred using L_m, as in (19). So by rearranging (19) and doing some simplifications, the DCM voltage gain can be calculated as follows:

$$M_{\text{DCM}} = \frac{V_{\text{out}}}{V_{\text{in}}} = D_{Qa} \sqrt{\frac{R_o}{2 L_m f}}. \tag{36}$$

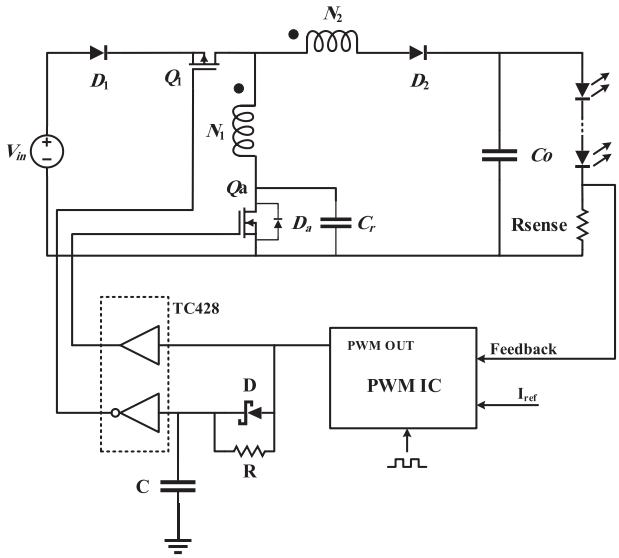

Fig. 5. General control method of the proposed LED driver.

E. Voltage Stress

The maximum reverse voltage endured by the main switch is equal to

$$V_{Q1} = V_{in} + \frac{V_o}{n-1}. \tag{37}$$

The voltage stress across the auxiliary switch is equal to the maximum voltage of C_r which can be derived from (21)

$$V_{Qa} = V_{Cr-\max}. \tag{38}$$

Maximum reverse voltage across the input and output diodes are

$$V_{D1} = \frac{V_o}{n-1} \tag{39}$$

$$V_{D2} = V_o + (n-1) V_{\text{in}}. \tag{40}$$

IV. Control Method

One of the advantages of this proposed LED driver is that the added auxiliary switch for creating soft switching condition does not impose driving circuit complexity. The general control methodology can be observed in Fig. 5 that the LED string current is sensed by the R_{sense} and is compared with a reference value in a PWM IC which regulates the output pulsewidth . Since both switches turn ON simultaneously and the main switch would remain ON for a fixed portion of time after the auxiliary switch turns OFF, they can both be driven with one driving signal. In this scheme, the main switch is a p-channel MOSFET and the auxiliary switch is an n-channel one. The required duty cycle produced by PWM IC is adjusted for the auxiliary switch which controls the output power, and the output PWM pulse is amplified via a current buffer and drives the auxiliary switch. This same pulse is also amplified and applied to drive the main switch, so both switches trigger on at the same time. When the driving signal becomes low, Q_a is turned OFF, but, Q_1 should remain ON for a specific portion of time. This time delay is produced by the

TABLE I
COMPARISON BETWEEN THE PROPOSED CONVERTERS AND THOSE PRESENTED IN [17]–[19]

Symbol	[17]	[18]	[19]	Proposed converter	Proposed converter (without input diode)
Number of Switches	1	2	2	2	2
Soft switching	Yes	Yes	No	Yes	Yes
Number of magnetic cores	2	1	2	1	1
Efficiency at 26W output power	93%	89.5%	93.1%	90.3%	92.9%

TABLE II
ELEMENTS USED FOR THE IMPLEMENTED PROTOTYPE

Parameter	Symbol	Value
Input voltage	V_{in}	12V
Output voltage	V_{out}	32V
Output power	P_{out}	26W
Switching frequency	f	100kHz
Magnetizing inductance	L_m	5μH
Turns ratio	n	3
Main switch	Q_1	SUM110P06-08L
Auxiliary switch	Q_a	SQJA04EP
Input diode	D_1	V15P45S-M3
Output diode	D_2	V8P10
Resonant capacitor	C_r	47nf/50V
Output capacitor	C_o	10μf/50V

added RC circuit which is designed based on the required delay. This way, after Q_a is switched OFF, the RC circuit keep Q_1 ON for the required time delay.

V. PERFORMANCE COMPARISON

The proposed converter is compared with some other similar drivers presented in [17]–[19] as can be observed in Table I. Compared to [17], although the proposed converter has an extra switch, but only one magnetic core is incorporated which decreases the circuit volume and weight. In addition, the auxiliary switch in the proposed converter provides soft switching condition for both switches. But, in converter of [17], the switch turns OFF under hard switching condition. Furthermore, the inductor used in series with switch, causes voltage spike at switch turn OFF. In the proposed converter, both switches can be driven with a simple gate driver by employing p-type MOSFET along with the n-type. Compared with [19], the proposed converter has the advantages of soft switching performance and fewer magnetic cores. Although the proposed converter and the converter presented in [18] have the same number of switches and magnetic cores and both feature soft switching performance, the proposed converter possesses simpler gate drive and also, power is processed twice in [18]. Also, the efficiency of the proposed converter is compared with the ones presented in [17]–[19] using simulation analysis in PSPICE software under the same operating condition. Input voltage is 12 V, output voltage is 32 V, output power is 26 W, and the operating frequency is 100 kHz. Exactly the same power MOSFETs and diodes are used for all the converters so that the comparison would be completely fair. IRF540 is used as MOSFETs and MBR3045CT is selected for diodes. Only inductor and capacitor losses are ignored since these losses are relatively small. Also, it should be noted that the semiconductors used for the implemented prototype were not available in PSPICE libraries, so alternative elements were chosen in simulation analysis. As can be observed in Table I, converters proposed in [17] and [19] and the proposed converter without the input diode, have almost the same efficiency, and converter in [18] has the lowest efficiency among the converter. If the output load is fixed, the input diode can be omitted from the proposed converter which improves the overall efficiency by about 2.6%. But, regarding the application for which the converter is designed, LED 7-segment displaying different digits, the output load varies, and at light loads, a small portion of power returns to the input battery. Thus, the input diode is maintained to prevent any potential damage to the input battery. It should be noted that even with the input diode remaining, the proposed converter still has high efficiency. Converters presented in [17]–[19] operate in CCM which leads to larger inductors in comparison with the proposed converter which operates in DCM and uses a small inductor. Operation in CCM would result in reduced conduction losses, but at the cost of larger inductors. Also, converters [17] and [19] use two separate magnetic cores which increases size, volume, and losses, while the proposed converter uses a single magnetic element.

VI. EXPERIMENTAL RESULTS

In order to evaluate the effectiveness of the proposed scheme in practical condition, a laboratory prototype of the proposed converter is implemented. The input voltage, as the standard value of the batteries, is 12 V which is converted to 32 V at 26 W output power. The switching frequency is selected 100 kHz. From (20), the value of the magnetizing inductance is calculated 5 μH and from (35) C_r is 47 nF/50 V. The input diode is V15P45S-M3 while D_2 is selected V8P10. From (25), (28), and (32), n is selected 3. The main switch is SUM110P06-08L and the auxiliary switch is SQJA04EP. Complete specifications of the implemented prototype are listed in Table II.

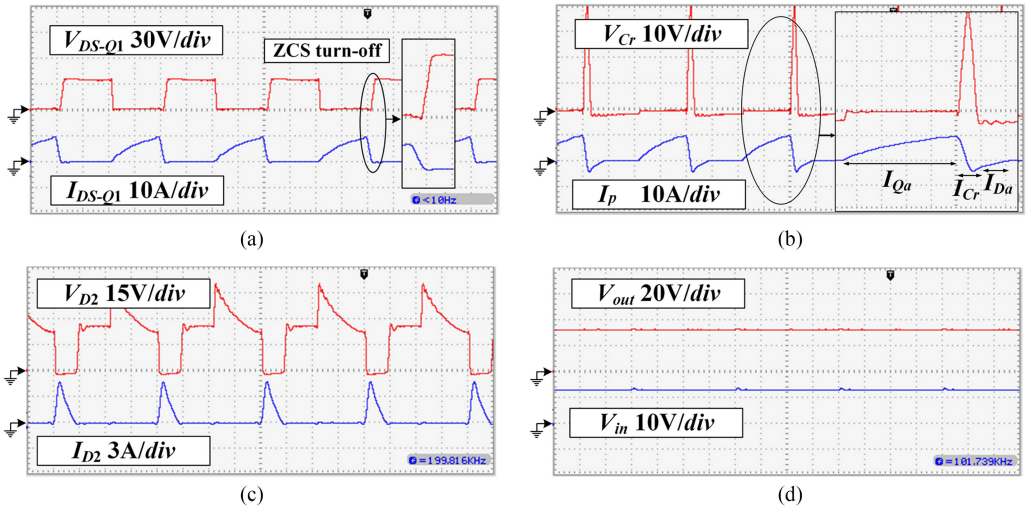

Fig. 6. Experimental results of the prototype converter. (a) VDS-Q1, IDS-Q1. (b) VCr, Ip. (c) VD2, ID2. (d) Vout, Vin (2.5 μs).

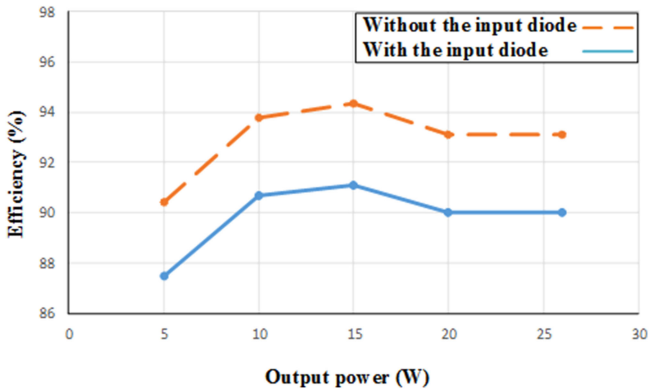

Fig. 7. Efficiency of the proposed LED driver.

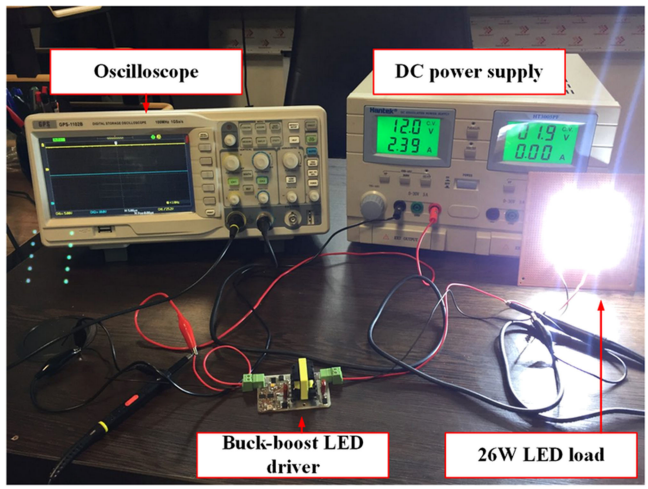

Fig. 8. Photograph of the implemented proposed LED driver.

The drain-source voltage of the main switch Q_1 as well as its drain-source current waveform is shown in Fig. 6(a). As can be seen, before turn-OFF instant, drain-source current descends to zero then Q_1 drain-source voltage begins to increase, so, ZCS condition is realized for Q_1 which considerably decrease switching losses. The voltage stress across Q_1 is almost equal to the output voltage. Since, Q_1 current is identical to the D_1 current, ZCS turn OFF for both Q_1 and D_1 is achieved and no reverse recovery is observed for D_1. The primary side current (I_p) along with C_r voltage which is the same as Q_a voltage, are shown in Fig. 6(b). As can be observed, due to the primary leakage inductance, the current increase in Q_a which is the same as I_p is gradual and this switch turns ON softly. Also, the Q_a antiparallel diode, D_a, turns OFF under ZCS which removes the reverse recovery losses of this diode. Also, when Q_a triggers on, C_r is fully discharged, so, Q_a turns ON under ZVS condition. The voltage and current waveforms of the output diode, D_2, are depicted in Fig. 6(c) which shows ZCS turn ON and turn OFF of D_2 which has eliminated the reverse recovery losses. The input and output voltage waveforms are observable in Fig. 6(d). A uniform constant voltage is provided for LEDs at the output, and the boost topology provides enough voltage for multiple LEDs in series and parallel configurations even when the input voltage level is insufficient. The efficiency of the proposed converter is shown Fig. 7. The achieved efficiency for the proposed converter with the input diode is 90% at nominal load, and the achieved efficiency at full load condition for the proposed converter without the input diode is 93.1%. As mentioned before, because of the variable output LED load, the input diode is maintained in order to prevent any returned power to the input battery.

The experimental setup is shown in Fig. 8.

VII. Conclusion

A buck–boost type dc–dc converter for battery driven LED driving applications is presented in this paper. A resonance circuit consisting of the magnetizing and leakage inductance of the coupled inductors and a capacitor paralleled with an active switch is employed to create ZCS condition for the main switch ZVS for the auxiliary switch which reduces switching losses. One magnetic element is utilized in this converter which

simplifies the circuit structure. All diodes turn OFF at ZCS and the associated reverse recovery losses are alleviated. The proposed LED driver can perform in both buck and boost modes, and can provide the required voltage for LEDs with different colors. Having simple structure, low component count, soft switching performance, and buck and boost mode flexibility make this converter a good candidate for LED drive applications where the input voltage source and available space are limited, high efficiency is required and LEDs with different colors can be driven. The experimental results show satisfactory performance of the proposed scheme in practical use.

REFERENCES

[1] W. Yu, J. S. Lai, H. Ma, and C. Zheng, "High-efficiency DC–DC converter with twin bus for dimmable LED lighting," *IEEE Trans. Power Electron.*, vol. 26, no. 8, pp. 2095–2100, Aug. 2011.

[2] X. Wu, C. Hu, J. Zhang, and C. Zhao, "Series–parallel autoregulated charge-balancing rectifier for multioutput Light-Emitting Diode driver," *IEEE Trans. Ind. Electron*, vol. 61, no. 3, pp. 1262–1268, Mar. 2014.

[3] J. Zhang, J. Wang, and X. Wu, "A capacitor-isolated LED driver with inherent current balance capability," *IEEE Trans. Ind. Electron.*, vol. 59, no. 4, pp. 1708–1716, Apr. 2012.

[4] Y. Lu, D. Czarkowski, and W. E. Bury, "High efficiency adaptive boost converter for LED drivers," in *Proc. 7th Int. Conf.-Workshop Compat. Power Electron.*, Tallinn, Estonia, 2011, pp. 315–318.

[5] Y. Chen, Y. Nan, S. Zhong, and Q. Kong, "An input-adaptive self-oscillating synchronous boost converter for LED driving with ultra-low wide-range voltage input," *IEEE Energy Convers. Congr. Expo.*, Pittsburgh, PA, USA, 2014, pp. 5243–5248.

[6] X. Xu and X. Wu, "High dimming ratio LED driver with fast transient boost converter," in *Proc. IEEE Power Electron. Spec. Conf.*, Rhodes, Greece, 2008, pp. 4192–4195.

[7] M. R. Amini, A. Emrani, E. Adib, and H. Farzanehfard, "Single soft switched isolated converter with constant output current for light emitting diode driver," *IET Power Electron.*, vol. 7, no. 12, pp. 3110–3115, 2014.

[8] J. Garcia, A. J. Calleja, E. L. Corominas, D. G. Vaquero, and L. Campa, "Interleaved buck converter for fast PWM dimming of high-brightness LEDs," *IEEE Trans. Power Electron.*, vol. 26, no. 9, pp. 2627–2636, Sep. 2011.

[9] Y. Chen, Y. Nan, and Q. Kong, "A loss-adaptive self-oscillating buck converter for LED driving," *IEEE Trans. Power Electron.*, vol. 27, no. 10, pp. 4321–4328, Oct. 2012.

[10] X. Qu, S. C. Wong, and C. K. Tse, "Resonance-assisted buck converter for offline driving of power LED replacement lamps," *IEEE Trans. Power Electron.*, vol. 26, no. 2, pp. 532–540, Feb. 2011.

[11] J. Zhang, T. Jiang, and X. Wu, "A high-efficiency quasi-two-stage LED driver with multichannel outputs," *IEEE Trans. Ind. Electron.*, vol. 64, no. 7, pp. 5875–5882, Jul. 2017.

[12] Q. Hu and R. Zane, "Minimizing required energy storage in off-line LED drivers based on series-input converter modules," *IEEE Trans. Power Electron.*, vol. 26, no. 10, pp. 2887–2895, Oct. 2011.

[13] Y. Lu, D. Czarkowski, and W. E. Bury, "High efficiency adaptive boost converter for LED drivers," in *Proc. 7th Int. Conf.-Workshop Compat. Power Electron.*, Tallinn, Estonia, 2011, pp. 315–318.

[14] J. i. Kang, J. Han, and S. K. Han, "High-efficiency boundary conduction mode tapped-inductor boost LED driver," in *Proc. IEEE Int. Conf. Ind. Technol.*, Busan, South Korea, 2014, pp. 261–266.

[15] R. Kathiresan, T. M. Xiong, S. K. Panda, P. Das, and T. Reindl, "A non-isolated converter design with time-multiplexing control topology for unbinned high-power LEDs in parallel operation for off-grid solar-PV street-lamps," in *Proc. IEEE Int. Conf. Sustain. Energy Technol.*, Hanoi, Vietnam, 2016, pp. 359–363.

[16] X. Xu and X. Wu, "High dimming ratio LED driver with fast transient boost converter," in *Proc. IEEE Power Electron. Spec. Conf.*, Rhodes, Greece, 2008, pp. 4192–4195.

[17] S. W. Lee, H. J. Choe, and J. J. Yun, "Performance improvement of a boost LED driver with high voltage gain for edge-lit LED backlights," *IEEE Trans. Circuits Syst. II, Exp. Briefs*, vol. 65, no. 4, pp. 481–485, Apr. 2018.

[18] K. I. Hwu and W. Z. Jiang, "Nonisolated two-channel LED driver with automatic current balance and zero-voltage switching," *IEEE Trans. Power Electron.*, vol. 31, no. 12, pp. 8359–8370, Dec. 2016.

[19] K. I. Hwu and W. Z. Jiang, "Non-isolated two-phase interleaved LED driver with capacitive current sharing," *IEEE Trans. Power Electron.*, vol. 33, no. 3, pp. 2295–2306, Mar. 2018.

[20] M. Jabbari and H. Farzanehfard, "Family of soft-switching resonant DC-DC converters," *IET Power Electron.*, vol. 2, no. 2, pp. 113–124, Mar. 2009.

Authors' photographs and biographies not available at the time of publication.